34th Annual International Conference of the IEEE EMBS
San Diego, California USA, 28 August - 1 September, 2012

Patient Specific Multiscale Modelling for Plaque Formation and Progression

T.P. Exarchos, *Member, IEEE,* A. Sakellarios, P.K. Siogkas, D.I. Fotiadis, *Senior Member, IEEE,* Z. Milosevic, D. Nikolic, N. Filipovic, *Member, IEEE,* P. Marraccini, F. Vozzi, O. Parodi

Abstract—**We present a three-dimensional model of plaque formation and progression that was tested in a set of patients who underwent coronary Computed Tomography angiography (CTA) for anginal symptoms. The 3D blood flow is described by the Navier-Stokes equations, together with the continuity equation. Mass transfer within the blood lumen and through the arterial wall is coupled with the blood flow and is modeled by a convection-diffusion equation. The Low Density Lipoprotein (LDL) transports in lumen of the vessel and through the vessel tissue (which has a mass consumption term) are coupled by Kedem-Katchalsky equations. The inflammatory process is modeled using three additional reaction-diffusion partial differential equations. A full three-dimensional model was created. Furthermore, features potentially affecting plaque growth, such as patient risk score, circulating biomarkers, localization and composition of the initial plaque, and coronary vasodilating capability were also investigated. The proof of concept of the model effectiveness was assessed 6 months after the baseline evaluation.**

I. Introduction

Low endothelial wall shear stress (WSS) promotes the development of early fibroatheromas, the evolution of which follows an individualized natural history of progression. In-vivo assessment of the local WSS, extent of vascular inflammation and arterial remodeling response which are all responsible for individual plaque evolution, in combination with systemic biomarkers of vascular inflammation, may all together improve risk stratification of individual early atherosclerotic plaques, thereby personalizing the therapeutic strategies. Although noninvasive imaging and coronary angiography are still unable to identify plaque evolution and propensity for future instability, novel approaches, such as local WSS dependent accumulation of inflammatory cells in specific vascular regions [1] has been derived by computational fluid dynamics (CFD) and mass transfer methods [2]. CFD methods based on in vivo three-dimensional vessel reconstruction have recently been introduced to assess the influence of WSS on altered endothelial cells as well as on vascular smooth muscle cells, that could potentially furnish patient-specific fingerprints for risk stratification of a vascular lesion.

The heterogeneity of plaque distribution and progression, despite the exposure of the arterial vasculature to the same systemic risk factors, claims attention towards geometrical conditions and hemodynamic forces that may locally favor disturbed or low WSS [3, 4]. Today, noninvasive techniques such as coronary Computed Tomography angiography (CTA) [5] or phase contrast Magnetic Resonance imaging [6] can reliably be employed for CFD evaluations. Long et al. [7] managed to reconstruct carotid bifurcations including the lumen, the arterial wall as well as the atheromatic plaque segments using MR images, in order to identify the impact of the arterial geometry on the generated stresses of the artery. Tang et al. [8] created 3D models of human carotid arteries, incorporating all types of atheromatic plaque to investigate critical flow conditions as well as the generated stress/strain values during those conditions and examine their correlation to plaque rupture. In another study of the same group [9], 3D multicomponent models of carotid bifurcations were created to examine the possible correlation of intraplaque hemorrhage and shear stresses.

In the present study, a group of patients with coronary artery disease (CAD) and intermediate lesions was evaluated by CTA, and an innovative approach to simulate the WSS-related LDL transport across the endothelium and to identify LDL accumulation sites was used. The novelty of this work lies in the acquisition of systemic factors related to atherosclerosis evolution (risk profile, inflammation), measurements of coronary microcirculatory vasodilating capability, and the systematic verification of prediction of plaque progression by repeated CTA, six months after the baseline evaluation.

II. Multiscale Modelling

A. 3D arterial tree reconstruction

For the 3D reconstruction of an arterial tree using CTA images, the following approach is followed:
In the first stage of the reconstruction algorithm, the axial images are stacked into a 3D data cube. This stage comprises

Manuscript received March 15, 2012. This work was supported by the EU project ARTreat FP7-224297, Multi-level patient-specific artery and atherogenesis model for outcome prediction, decision support treatment, and virtual hand-on training.

T.P. Exarchos, P.K. Siogkas and D.I. Fotiadis are with the Foundation for Research and Technology Hellas, Institute of Molecular Biology and Biotechnology, University of Ioannina, Ioannina, GR 45110, Greece; e-mail: exarchos@cc.uoi.gr, psiogkas@cc.uoi.gr, fotiadis@cc.uoi.gr).

A. Sakellarios and D.I. Fotiadis are with the Unit of Medical Technology and Intelligent Information Systems, Dept. of Materials Science and Enginnering, University of Ioannina, Ioannina, GR 45110, Greece (e-mail: ansakel@cc.uoi.gr).

Z. Milosevic, D. Nikolic, N. Filipovic are with the University of Kragujevac, Serbia (e-mail: zarko@kg.ac.rs, markovac85@kg.ac.rs, fica@kg.ac.rs)

P. Marraccini, F. Vozzi and O. Parodi is with the Instituto di Fisiologia Clinica, Consiglio Nazionale delle Ricerche, Pisa, Italy (email: oberpar@tin.it)

four steps: 3D data volume creation, selection of region of interest (ROI), extraction of binary images and filtering of the binary images. In particular, a first initial 3D data cube V_{in} from the set of N axial images (i,j,k) is created as:

$$V_{in}(i,j,k) = I_k(i,j). \quad (1)$$

where I_k is the k^{th} axial image.

Next, the region of interest, which is the particular region of heart including the coronary arteries, is selected. The new set of grey scale images includes also other components such as the pulmonary arteries and aorta. Then, the images are converted to binary by replacing all pixels with brightness greater than a specified limit with the value one (white), and all other pixels with the value zero (black). Finally, the binary images are filtered in order to make easier the detection of the coronary arteries. To achieve this, we assume that very small and very large objects in each image should be excluded. Each object is segmented, each area is calculated and the undesirable objects are excluded.

The next stage of the algorithm is the automated reconstruction of the arterial tree. Initially, the objects are identified in the images creating two 3D data cubes (right and left coronary arterial tree). Object identification is achieved by identifying which voxels are connected and assigning the same label on them. Then, label equivalences are recorded using the 26-connected neighborhood connectivity. In this scheme, two "on" voxels are considered connected if the following condition is valid: two voxels share either one common face (6 options) or one common edge (12 options) or one common corner (8 options). Label equivalences are recorded in a union find table and equivalence classes are resolved using the union-find algorithm [10]. The output of this subroutine is a new 3D data cube, within which all objects, including the two coronary arteries are labeled, thus the segmentation of the desired objects is straight-forward, as long as their labels are known. Then, connection of the arterial branches is performed and the arterial tree is reconstructed. First, the initial 3D data cube is processed in order to distinguish the branches and store them separately in different data cubes. The subroutine which performs the separation of the branches includes ramification detection, single-branch data cubes creation and cubes refinement.

From the previous procedure 3D cubes that contain only one branch are generated. Finally, a thinning algorithm [11] is applied to extract the centerline and then active contours are used [12] and the resulting points of the deformation represent the border of the coronary artery in that frame.

In order to create the cloud point for each branch, the axial CT images are converted to be parallel to the vertical axes. The main steps of the algorithm which creates the point cloud are the extraction of lines perpendicular to centerline, the extraction of projected border lines and the nodes extraction. Finally, the cloud points of desired number of branches is fused to create one arterial tree.

B. Blood flow modelling

The blood flow in the domain defined by the lumen, is modeled by the Navier-Stokes equations, together with the continuity equation for incompressible fluids:

$$\rho * \partial \mathbf{u}_l / \partial t - \mu \nabla^2 \mathbf{u}_l + \rho(\mathbf{u}_l \cdot \nabla)\mathbf{u}_l + \nabla p_l = 0, \quad (3)$$

$$\nabla \cdot \mathbf{u}_l = 0, \quad (4)$$

where l refers to the lumen, $\mathbf{u}_l$ is the blood velocity, p_l is the pressure, μ is the dynamic viscosity of blood, and ρ is the blood density [13]. Blood velocity and pressure are taken from the patient-specific measurements. Mass transfer in the blood is coupled with the blood flow and is modeled by the convection-diffusion equation:

$$\nabla \cdot (-D_l \nabla c_l + c_l \mathbf{u}_l) = -\partial c_l / \partial t, \quad (5)$$

in the fluid domain, where c_l is the solute concentration in the blood, and D_l is the solute diffusivity in the lumen. In addition to the velocity field, the wall shear stress computation is performed. The mean shear stress within a time interval T is calculated as [14]:

$$\tau_{mean} = \left| \frac{1}{T} \int_0^T \mathbf{t}_s dt \right|, \quad (6)$$

where $\mathbf{t}_s$ is the scalar traction component parallel to the vessel axis. Another scalar quantity is a time-averaged magnitude of the surface traction vector, calculated as

$$\tau_{mag} = \frac{1}{T} \int_0^T |\mathbf{t}_s| dt. \quad (7)$$

The oscillatory shear index (OSI) is defined as [15]:

$$OSI = \frac{1}{2}\left(1 - \frac{\tau_{mean}}{\tau_{mag}}\right). \quad (8)$$

C. Mass transfer modelling

Mass transfer in the arterial wall is coupled to the transmural flow and is modeled by a convection-diffusion-reaction equation as follows:

$$\nabla \cdot (-D_w \nabla c_w + k c_w u_w) = r_w c_w \quad (9)$$

where c_w is the solute concentration and D_w is the solute diffusivity in the arterial wall; u_w is the plasma velocity in the wall, K is the solute lag coefficient, and r_w is the consumption rate constant. The mass transport in the lumen and in the vessel wall are coupled by the Kedem-Katchalsky equations:

$$J_v = L_p(\Delta p - \sigma_d \Delta \pi), \quad (10)$$

$$J_s = P \Delta c + (1 - \sigma_f) J_v \bar{c}, \quad (11)$$

where L_p is the hydraulic conductivity of the endothelium; Δc is the solute concentration difference, Δp is the pressure drop and $\Delta \pi$ is the oncotic pressure difference, in the endothelium; σ_d is the osmotic reflection coefficient, σ_f is the solvent reflection coefficient, P is the solute

endothelial permeability, and $\bar{c}$ is the mean endothelial concentration. The first term in the Kedem-Katchalsky equations $P\Delta c$ of the right hand side in Eq. (11) defines the diffusive flux across the endothelium, while the second term $(1-\sigma_f)J_v\bar{c}$ defines the convective flux. Only the oncotic pressure difference $\Delta\pi$ is neglected in our simulations because of the decoupling of the fluid dynamics from the solute dynamics. The above equations are transformed into a finite element system of incremental-iterative equations and is solved over several time steps.

The atherosclerotic process starts with the accumulation of LDL in the intima, where part of it is oxidized and becomes pathological. In order to remove the oxidized particles, circulating immune cells (e.g. monocytes) are recruited. Once in the intima, the monocytes differentiate and become macrophages that phagocyte the oxidized LDL. Fatty macrophages then transform into foam cells. Foam cells are responsible for the growth of a subendothelial plaque which eventually emerges to the artery lumen. The inflammatory process is modeled using three additional reaction-diffusion partial differential equations [16]:

$$\partial_t O = d_1\Delta O - k_1 O\cdot M,$$
$$\partial_t M + div(v_w M) = d_2\Delta M - k_1 O\cdot M + S/(1+S), \quad (12)$$
$$\partial_t S = d_3\Delta S - \lambda S + k_1 Ox\cdot M + \gamma(O - O^{thr}),$$

where O is the oxidized LDL in the wall, M and S are concentrations in the intima of macrophages and cytokines, respectively; d_1, d_2, d_3 are the corresponding diffusion coefficients; λ and γ are the degradation and LDL oxidized detection coefficients; and v_w is the inflammatory velocity of plaque growth, which satisfies Darcy's law and the incompressibility continuity equation [17]:

$$v_w - \nabla\cdot(p_w) = 0, \quad (13)$$
$$\nabla v_w = 0, \quad (14)$$

in the wall domain. p_w is the pressure in the arterial wall. In order to follow the change of the vessel wall geometry during plaque growth, a 3D mesh moving algorithm Arbitrary Lagrangian Eulerian, (ALE) is used [18].

For plaque volume progression we need at least two different points in time from medical images. We use the following equations:

$$F_{t_{n(k+1)}}(i,j) = p_0(j) + p_1(j) * F_{t_{n(k)}}(i,j) + p_2(j)$$
$$* \left.\frac{dF_{t_{n(k)}}(i,j)}{dt}\right|_{t_n} * \Delta t + p_3(j) * \left.\frac{d\tau^{wss}{}_{t_{n(k)}}(i,j)}{dt}\right|_{t_n} * \Delta t, \quad (15)$$

where $F_{t_{n(k+1)}}(i,j)$ is function of the coordinate of wall thickness I for cross section j at time tn, k is iteration, $k=0,1,2,3\ldots$; n is the time point for image data, $p(0),p(1),\ldots$are coefficients, τwss is the wall shear stress, Δt is the time step. A simple linear regression analysis using least squares is used for the estimation of the coefficient $p(0), p(1)\ldots$ for each specific patient.

III. Results

Fig. 1 presents the baseline and follow-up after 6 months models for one patient case. It is evident that the influence of WSS was observed on this patient in the distal portion of the circumflex artery, that showed a marked progression of the baseline stenosis. Location of the lowest WSS (Fig. 1a) in the distal portion of the vessel corresponded to the site of plaque growth after 6 months (Fig. 1b). CFD data were used as input for a fitting procedure of volume plaque progression. Oxidized LDL distribution at baseline and follow-up study after 6 months in this patient case is shown in Fig. 2. It can be observed that after 6 months there is a significant increase in LDL distribution distal from the most narrowed part of the lumen domain. Due to complex lumen and wall domain, only the LDL distribution for the joint boundaries is presented in Fig. 2.

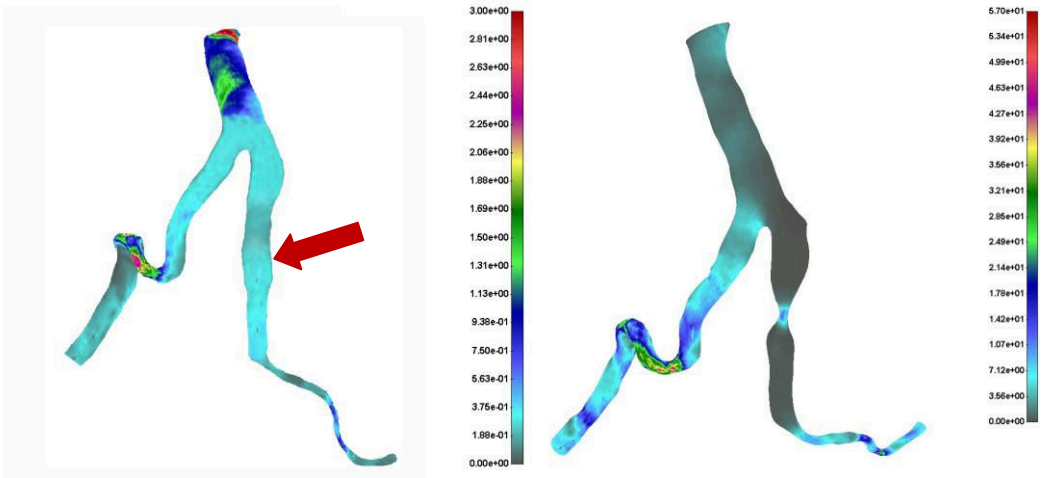

Fig. 1: Local shear stress distribution at baseline (A) and after 6 months follow-up (B) in one patient case. Area with plaque progression at follow-up towards critical stenosis (distal circumflex artery) showed at baseline the lowest shear stress value (arrow). Wall shear stress values are expressed in [Pa] units.

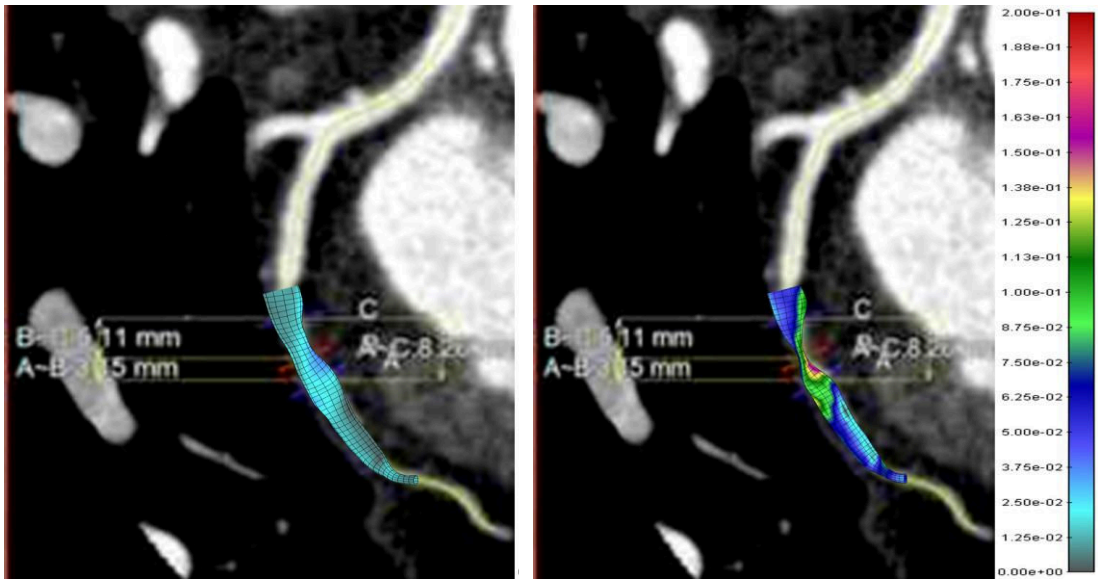

Fig. 2: LDL distribution at baseline and in the follow-up study in the distal circumflex artery with obvious lumen diameter reduction. Angiography slices are depicted as background of the computer simulation results. Units for LDL concentration [mg/ml].

IV. Discussion

A multiscale model for the biological process of plaque formation and progression has been applied to CTA imaging in patients with non obstructive coronary plaques. The model includes the 3D reconstructed arterial model, the blood flow, the WSS distribution, the molecular/cell model mechanism involved in the generation and growth of atherosclerotic plaque. The governing partial differential equations for plaque formation rely on the mass balance and the Darcy's law in the domain of plaque development; the Navier-Stokes and diffusion equations are used for the LDL transport within the arterial lumen; the transport-diffusion-reaction equations are employed for the transmural mass transport, including the Kedem-Katchalsky equations to couple the transmural and transport within the lumen.

References

[1] H. M. Honda, T. Hsiai, C. M. Wortham, M. Chen, H. Lin, M. Navab, L. L. Demer. "A complex flow pattern of low shear stress and flow reversal promotes monocyte binding to endothelial cells," *Atherosclerosis*, Vol. 158, no. 385, pp. 390, 2001.

[2] U. Olgac, V. Kurtcuoglu, D. Poulikakos. "Computational modeling of coupled blood-wall mass transport of LDL: effects of local wall shear stress," *Am. J. Physiol. Heart Circ Physiol*., Vol. 294, no. 2, pp. H909–919, 2008.

[3] Y. S. Chatzizisis, A. U. Coskun, M. Jonas, E. R. Edelman, C. L. Feldman, P. H. Stone. "Role of endothelial shear stress in the natural history of coronary atherosclerosis and vascular remodeling: molecular, cellular and vascular behavior," *J Am Coll Cardiol*., Vol. 49, pp. 2379 –2393, 2007.

[4] Y. S. Chatzizisis, M. Jonas, A. U. Coskun, R. Beigel, B. V. Stone, C. Maynard, R. S. Gerrity, W. Daley, C. Rogers, E. R. Edelman, C. L. Feldman, P. H. Stone. "Prediction of the localization of high risk coronary atherosclerotic plaques on the basis of low endothelial shear stress: an intravascular ultrasound and histopathology natural history study," *Circulation*, Vol. 117, pp. 993–1002, 2008.

[5] T. Wischgoll, J. S. Choy, G. S. Kassab. "Extraction of morphometry and branching angles of porcine coronary arterial tree from CT images," *Am J Physiol Heart Circ Physiol.*, Vol. 297, pp. H1949–H1955, 2009.

[6] H. Gao, Q. Long, M. Graves, J. H. Gillard, Z. Y. Li. "Carotid arterial plaque stress analysis using fluid–structure interactive simulation based on in-vivo magnetic resonance images of four patients," *Journal of Biomechanics,* Vol. 42, pp. 1416–1423, 2009.

[7] H. Gao, Q. Long, M. Graves, J.H. Gillard, Z.-Y. Li. "Study of reproducibility of human arterial plaque reconstruction and its effects on stress analysis based on multispectral in vivo magnetic resonance imaging," *Journal of MRI,* Vol. 30, no.1, pp. 85-93, 2009.

[8] D. Tang, C. Yang, J. Zheng, P.K. Woodard, G.A. Sicard, J.E. Saffitz, C. Yuan. "3D MRI-based multicomponent FSI models for atherosclerotic plaques," *Annals of Biom. Engineering,* vol. 32, pp. 947-960, 2004.

[9] X. Huang, Z. Teng, G. Canton, M. Ferguson, C. Yuan, D. Tang. "Intraplaque hemorrhage is associated with higher structural stresses in human atherosclerotic plaques: An in vivo MRI-based 3d fluid-structure interaction study," *BioMed. Eng. On.*, Vol. 9, art. no. 86, 2010

[10] S. Ulzheimer, W.A. Kalender, "Assessment of calcium scoring performance in cardiac computed tomography," *Eur Radiol,* Vol.13(3), pp.484-497, 2003.

[11] L. Huang, "An Improved Parallel Thinning Algorithm." *Proceedings of the Seventh International Conference on Document Analysis and Recognition* (ICDAR). 2003.

[12] C. Xu, J. L. Prince, "Snakes, shapes, and gradient vector flow." *IEEE Transactions on Image Processing.* 1998, Vol. 7, 3, pp. 359-369.

[13] S. Schroeder, A.F. Kopp, A. Baumbach, C. Meisner, A. Kuettner, C. Georg, B. Ohnesorge, C. Herdeg, C.D. Claussen, K.R. Karsch, "Noninvasive detection and evaluation of atherosclerotic coronary plaques with multislice computed tomography," *J Am Coll Cardiol,* vol. 37, no. 5, pp. 1430-1435, 2001.

[14] M. Prokop, M. Galanski, A.J. van der Molen, C. Schaefer-Prokop, "Spiral and multislice computed tomography of the body," *Thieme*, New York, 2003.

[15] S.K. Mehta, J.R. McCrary, A.D. Frutkin, W.J. Dolla, S.P. Marso, "Intravascular ultrasound radiofrequency analysis of coronary atherosclerosis: an emerging technology for the assessment of vulnerable plaque," *Eur Heart J,* Vol. 28(11), pp.1283-1288, 2007.

[16] M. Kojic, N. Filipovic, B. Stojanovic, N. Kojic, "Computer Modeling in Bioengineering: Theoretical Background, Examples and Software," John Wiley and Sons, Chichester, England.

[17] V. Calvez, A. Ebde, N. Meunier, A. Raoult, "Mathematical modelling of the atherosclerotic plaque formation," *ESAIM Proc.*, Vol. 28, pp. 1-12, 2008.

[18] N. Filipovic, M. Rosic, I. Tanaskovic, Z. Milosevic, D. Nikolic, N. Zdravkovic, A. Peulic, M. Kojic, D. Fotiadis, O. Parodi, "ARTreat project: Three-dimensional Numerical Simulation of Plaque Formation and Development in the Arteries," *IEEE Transactions on Information Technology in BioMedicine* , 2011 (in press).